Catalytic hydrogen combustion using platinum supported on anodized aluminium oxide adhered to metallic aluminium

Stephanus P du Preez[a,*], Alina E Kozhukhova[a], and Dmitri G Bessarabov[a]

HySA Infrastructure, Faculty of Engineering, North-West University (NWU), Potchefstroom, South Africa

ABSTRACT

The implementation of catalytic hydrogen combustion (CHC) can mitigate the dependence on solid fuel combustion typically used in Sub-Saharan Africa as a means of heating. However, low-cost and readily available materials for catalyst fabrication are relatively unexplored. Considering the economic constraints regarding platinum group metals generally used for CHC, the cost of support materials and its functionalization as catalyst support has to be minimized. Typically, materials such as silicon carbide foam, extruded aluminium oxide-based ceramics, and titanium oxide mesh/sintered plates are used to withstand the high temperatures associated with CHC. In this paper, nanostructured anodized aluminium oxide (AAO) was synthesized as the support material via the anodization of high purity (>99%) aluminium (Al). The AAO layer intimately adhered to a metallic Al core acted as a thermal conduit to disperse heat throughout the catalyst. Platinum (Pt), considered as the reactive metal, was deposited to the AAO as nanoparticles with a diameter of approximately 19.3 nm. The CHC reaction proceeded spontaneously on the surface of the Pt/AAO catalyst. A combustion temperature of 408 ± 18 °C was maintained for 70 h at a 100 normal (N) mL min^{-1} hydrogen flow rate. The Pt-particles showed a relatively appreciable increase in particle size (from 19.3 nm to 25.0 nm), but the significance thereof was not evident during the 70 h CHC procedure.

KEYWORDS

anodized aluminium oxide, catalytic hydrogen combustion, metallic core

Received 09 April 2021, revised 24 November 2021, accepted 24 November 2021

INTRODUCTION

It is estimated that 2.8 billion people worldwide rely on the combustion of solid carbon fuel, resulting in 4 million premature deaths annually due to deaths related to poor domestic air quality.[1–3] Solid-carbon fuel combustion during household cooking and spatial heating is a serious health concern and can lead to various respiratory diseases and premature death.[1] Children and the elderly are more susceptible to such diseases;[4] children in households using solid fuels are more likely to develop pneumonia when compared to children in households that do not use solid fuels.[5–6] Also, particulate matter has been identified as one of the major pollutants and accumulates closer to the ground, making it easily inhaled by children under the age of 5 years.[7–8]

As an alternative and cleaner fuel, the use of hydrogen as an energy carrier is considered a suitable replacement for solid-carbon fuels. This consideration is mainly due to the occlusion of pollutant emissions, such as CO_x, SO_x, and particulate matter, during combustion.[9–10] The combustion reaction proceeds according to the following reaction:

$$H_2 + O_2 = H_2O,\ \Delta H = -57.9\ \text{kcal/mol} \quad (1)$$

Considering Reaction 1, hydrogen can be combusted in a confined space without consequential health implications as the only by-product is water. Hydrogen is produced via several processes, e.g., electrochemical,[11–15] photo-electrochemical,[16–17] photocatalytic,[18–19] photochemical,[20–21] thermochemical,[22–23], and various niche and biological processes.[24–32] Currently, the majority of hydrogen is produced from fossil fuels, and trace amounts of by-products such as CH_4, CO_2, and CO will be present.[33–34] Likely, the inclusion of the latter by-products will not appreciably affect the indoor air quality; CO is, however, a major health issue as exposure of more than 100 ppm is dangerous to human health.[35–37] Also, hydrogen produced from fossil fuels is not as accessible as electrochemically produced hydrogen when considering Sub-Saharan Africa. For instance, decentralized and small-scale electrolyzers operating on solar energy can be commissioned relatively easily as oppose to large steam-methane reformation plants.

It is not uncommon for electrical grids to be unstable or unavailable for extended periods in rural areas in developing countries, which in turn, negatively affects economic growth.[38] Typically, such rural areas rely on expensive diesel energy, pricing approximately $1 per kilowatt/hour (kWh), whereas solar energy is accessible at roughly $0.20 per kWh.[39] Therefore, it is evident that the utilization of solar power will benefit rural areas where electricity is not easily accessible. However, the utilization of renewable energy is curtailed by daily intermittence, e.g., periods of low wind speed and night.[40] Therefore, an approach to store energy is essential for uninterrupted electrical supply.[41] Several technologies exist, e.g., pumped hydro-storage, thermal energy, and batteries.[42] The latter technologies are generally employed on a small to medium scale and require relatively significant capital investment.

It is proposed that mini-grids be implemented, comprising a photovoltaic plant coupled with an electrolyzer. The electrolyzer can be supplied with excess energy to produce hydrogen from water. The electrolyzer can be scaled to meet a specific hydrogen output, determining the required energy input. Hydrogen has many uses, of which a comprehensive analysis is reported by Bessarabov and Millet.[43] Hydrogen is, however, typically supplied to a proton exchange membrane fuel cell (PEMFC) to convert the chemical energy of hydrogen into a current via Reaction 1. However, this approach is not feasible for heating purposes as a large PEMFC would be required to match the current required for heating. Therefore, hydrogen combustion is the most likely approach for heating applications.

A general shortcoming associated with direct (flame-based) hydrogen combustion includes the unintentional formation of toxic NO_x[44–45] which is minute at temperatures less than 800 °C and significant at more than 1400 °C.[45–46] Considering that the adiabatic flame temperature of hydrogen is between 2045 to 2127 °C,[47] NO_x formation is inevitable. Direct hydrogen combustion is further perplexed by flashbacks, which occur when hydrogen's laminar burning velocity exceeds the flow velocity of the hydrogen mixture.

Catalytic hydrogen combustion (CHC) is proposed as an alternative

*To whom correspondence should be addressed
Email: Faan.DuPreez@nwu.ac.za

ISSN 1996-840X Online / South African Chemical Institute / http://saci.co.za/journal

https://doi.org/10.17159/0379-4350/2022/v76a06

form of hydrogen combustion as this type of combustion prevents self-ignition and mitigates NO_x formation. It is achieved by controlling the combustion temperature below the temperature required for self-ignition (570 °C)[48–49] and NO_x formation. Several materials and devices have been developed for CHC for domestic applications. A recent review by Kozhukhova presents a summary of materials considerable for CHC. [50] Fumey et al. presented a CHC device based on a Pt/porous SiC foam catalyst; this device emitted ultra-low NO_x levels (8000 times below EU Regulations No. 813/2013).[46] However, the use of SiC foam is likely to lead to an increase in the cost of the catalyst. Du Preez et al. reported on the preparation of Pt supported on calcined stainless steel and Ti mesh for CHC.[41, 49] The Pt/stainless steel mesh showed signs of support degradation after prolonged combustion, and the Pt/Ti mesh may be considered economically impracticable due to the cost of the prefabricated Ti mesh.

Here we report on the synthesis of a Pt/anodized aluminium oxide (AAO) catalyst and its application in CHC. The benefits of using AAO as the support material include its low preparation cost (compared with other specialized materials). The Al substrate can be prefabricated to the desired shape before anodization.[51–52] Additionally, the presence of metallic Al at the catalyst core allows rapid thermal distribution from reaction sites via the intimately adhered AAO/metallic Al core boundary, reducing the likelihood of hot spots (defined as areas with a higher surface temperature than the average surface temperature).

MATERIALS AND METHODS

Pt/AAO catalyst synthesis

AAO supports were prepared by rapid two-step anodization of 10 × 10 mm Al (99.999%) sheets with a thickness of 0.25 mm. Before anodization, the surfaces of Al sheets were prepared as follows: degreased by ultra-sonication in acetone and deionized water, followed by electropolishing in a 1:4 v/v mixture of $HClO_4$ and ethanol at room temperature for 1 min at 20 V. The prepared Al sheets were thoroughly rinsed in deionized water. All anodization procedures were performed in a 0.4 M oxalic acid solution using a two-electrode electrochemical cell with a 5 × 15 cm stainless steel grid as the counter electrode. The oxalic acid solution was vigorously stirred during anodization, and isothermal conditions were maintained using a heating-refrigeration circulation system (Julabo, CORIO CD-200F, Germany). An adjustable power supply unit (RS PRO, IPS603, South Africa) was used as a DC power source for electropolishing and anodization procedures. The first anodization was performed at 40 °C and 30 V for 30 min. The initial AAO layer was removed using 5 vol% H_3PO_4/1.8 vol% CrO_3 at 60 °C for 45 min. The Al sheet was then reanodized at 45 V for 120 min. The difference in anodization potentials was implemented to reduce the anodization time to 120 minutes as several hours are typically used. The indicated rapid anodization procedure was considered in this study. The purpose was to prepare an AAO support, with limited emphasis on the morphological/structural properties of the obtained AAO.

Wet incipient impregnation was employed to prepare the Pt/AAO catalysts; Pt-precursor was introduced to the AAO support by submerging the supports in a 10 g L^{-1} chloroplatinic acid solution ($H_2PtCl_6.6H_2O$, Sigma Aldrich) for 10 s. AAO supports were then dried in ambient air and reduced in a 10/90 vol% H_2/N_2 atmosphere at 350 °C for 2 h to obtain nano-sized Pt particles. A heating rate of 5 °C min^{-1} was employed. A horizontal tube furnace was used to perform the reduction process (CTF12, Carbolite Gero, England).

The Pt and Al content of Pt/AAO catalyst was determined by inductively coupled plasma optic emission spectroscopy (ICP-OES). Before ICP-OES analysis, the AAO layer loaded with the Pt-precursor was dissolved in 5 vol% H_3PO_4/1.8 vol% CrO_3 at 60 °C for 45 min. The Pt loading was expressed as a function of the solubilized Al content, representing the AAO layer. Therefore, the metallic core was not included when calculating the Pt loading.

Catalytic hydrogen combustion evaluation

The catalytic activity of the Pt/AAO catalyst was evaluated in the ambient atmosphere. The catalyst was placed horizontally slightly above a 20 mm tube. High-purity hydrogen (99.9%) was supplied from an in-house developed hydrogen generator (Hydrogen South Africa Infrastructure, South Africa). The hydrogen was introduced at the bottom of the tube; the tube acted as a semi-enclosed environment for the hydrogen to be pre-mixed with air before reaching the catalyst surface. The hydrogen vol% concentration was estimated to be approximately 65% before combustion. A k-type thermocouple, coupled with an electronic data acquisition system, was placed at the centre of the catalyst surface. Temperature measurement was recorded every 1 s for the duration of all CHC reactions. Unreacted hydrogen was measured in the exhaust using a hydrogen sensor (Model XEN-5320, Xensor Integration, Netherlands). Reported temperatures were based on results obtained from three Pt/AAO catalysts. Each Pt/AAO catalyst was evaluated twice; average temperatures were reported unless specified otherwise.

Morphological and chemical characterization

Scanning electron microscopy was employed to characterize the morphology of AAO samples using an FEI Quanta FEG 250 field emission gun (Thermo Fisher Scientific, USA). Samples were placed on an Al stub using adhesive carbon tape and coated with a thin layer of carbon using a carbon coater (Emscope TB500, UK) before analyses. All AAO layer characterizations, i.e., layer thickness, pore diameter (D_p), interpore distance (D_c), were performed using ImageJ software. [53–54] The D_p value was calculated manually by measuring the visible pores. Similarly, for D_c, the distances between the centre of a pore and its neighbouring pore were manually measured. For D_c and D_p, 250 measurements were taken, and the average and standard deviation were reported.

Before and after CHC procedures, the Pt particle size was determined by transmission electron microscopy (TEM) by a Tecnai F20 FEI instrument (Thermo Fisher Scientific, USA). Before CHC, the Pt-containing AAO layer was mechanically separated, using a stainless steel blade, from the metallic core and extensively ultra-sonicated in acetone. After that, the Pt particle size was determined. After CHC procedures, a Pt/AAO catalyst was cross-sectioned by a focused ion beam (FIB). FIB lamellas were prepared by an FEI Helios Nanolab 650 dual-beam scanning microscope (Thermo Fisher Scientific, USA). TEM analyses were performed on the lamella to determine the Pt particle size.

RESULTS AND DISCUSSIONS

AAO support structure and morphology

Considering the risk of self-ignition of hydrogen if the surface temperature of the material used for CHC, it is essential to ensure that self-ignition is prevented. In some cases, the design of a CHC device does accommodate controlled self-ignition. For instance, Fumey et al. demonstrated a CHC device for cooking that can reach approximately 650 °C by controlled self-ignition of hydrogen between two porous sintered SiC disks.[55] However, this is not always the case, and the design of such a device is typically more complex and requires specialized materials. Therefore, the inclusion of the metallic core as a constituent of the Pt/AAO catalyst was considered as it mitigates the risk of self-ignition. Figure 1 shows a cross-sectioned AAO support and the surface thereof.

It is clear from Figure 1a that a thin metallic core of 5.0 ± 0.5 µm (based on 20 measurements taken every 15 µm over the length of the metallic core) was preserved after the anodization procedure used in this study. The AAO layer was approximately 100 µm thick on both sides of the metallic core. The metallic Al core has a thermal conductivity of approximately 237 W/m.K,[56] which is significantly higher than the thermal conductivity of alumina, i.e., 33 W/m.K.[57] Though the AAO (which consists of alumina) has a lower thermal conductivity than the

metallic Al core, it is assumed that due to the intimate contact between the AAO and the Al core, the thermal transfer limitations of the AAO layer are negligible.

Figure 1b shows that the AAO layer is relatively disorganized and consists of numerous pores, with diameters of 86.0 ± 9.4 nm and interpore distances of 108.7 ± 7.5 nm, as well as protruding nanowires. These nanowires form when the anodization procedure favours AAO dissolution over AAO formation. During AAO dissolution, pore walls are dissolved, and the corners of hexagonal cells remain intact.[51–52] It is further noted that the scope of this paper was to evaluate the use of AAO prepared from pure Al as catalyst support for CHC applications, and refinement of the AAO layer morphology was not considered.

Pt/AAO reactivity

Metal oxides are widely used as catalyst support materials, particularly for high-temperature combustion.[58–60] The use of Al_2O_3 is relatively widely reported; in some cases, Al_2O_3-supported catalysts used for various catalytic reactions are either pre-heated or require relatively extensive reaction initiation periods.[61–62] This is also true for CHC in some cases, and the catalyst or gas feed has to be pre-heated before CHC proceeds spontaneously.[41, 49, 63] The autocatalytic activity of the proposed Pt/AAO catalyst was investigated as it is considered an important property for various relevant catalyst applications, i.e., cooker and spatial heating. To evaluate this activity, the temperature profile of the Pt/AAO catalyst, with a Pt loading of 0.54 wt%, during its initial exposure to hydrogen was determined (Figure 2).

Figure 2 shows that the CHC reaction was spontaneous and initiated at an ambient temperature of 23 ± 4 °C after 25 ± 12 s of the catalyst being exposed to hydrogen (inset in Figure 2). A steady increase in the combustion temperature was observed for 150 s; this period was defined as the reaction initiation period. After that, the combustion temperature stabilized at 242 ± 3 °C (based on 1650 measurements). A relatively similar temperature profile was observed by Kozhukhova et al. [64], which is indicative of an active catalyst as no external energy is required to initiate the CHC reaction. A standard deviation of 7.6 to 106.4% was observed during the reaction initiation period, indicating that the values used to calculate the mean from which the standard deviation is calculated differed significantly. The observed deviation may be ascribed to the differences in the initial reaction temperate, i.e., 23 ± 4 °C. Therefore, the CHC reaction is highly temperature-sensitive, and a higher initial reaction temperature will greatly accelerate the combustion rate during the initial stages of CHC. The exothermic reaction heat self-catalyzes the CHC reaction and further expedite the combustion rate. The effects of lower initial reaction temperatures should be considered in future research.

After the combustion temperature stabilized at 242 ± 3 °C, the standard deviation did not exceed 9.8%. This temperature was maintained for the remainder of the 30 min CHC reaction. At a 40 NmL min^{-1} flow rate, the unreacted hydrogen content remained below 1 vol% after reaching the stable combustion temperature.

After the 30 min CHC reaction, three 6 h CHC reactions were performed to mimic the material's application during relatively extended periods of spatial heating. The 6 h heating period was selected as it represents a period from 12:00 pm to 06:00 am where the residential temperature of low-cost and informal dwellings in Johannesburg, South Africa, are at their lowest in May at 14 to 18 °C.[65] Figure 3 shows the average temperature profile of Pt/AAO for three 6h CHC reactions at a flow rate of 40 NmL min^{-1}. The average combustion temperature and standard deviation were calculated per hour for each of the three 6 h CHC reactions.

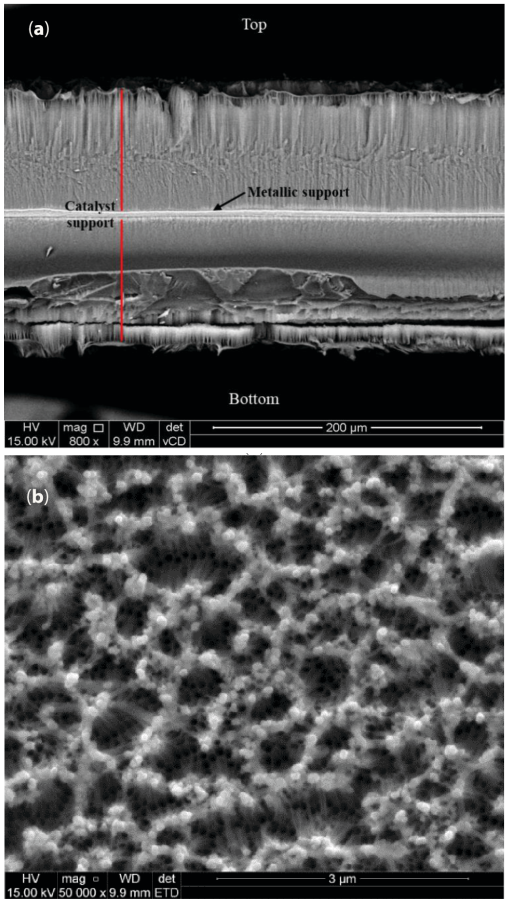

Figure 1: SEM micrographs of a manually cross-sectioned AAO support showing the metallic core and the AAO layer (indicated in red, a) prepared in back-scattered mode, and the surface morphology of the AAO layer (b) prepared in secondary mode

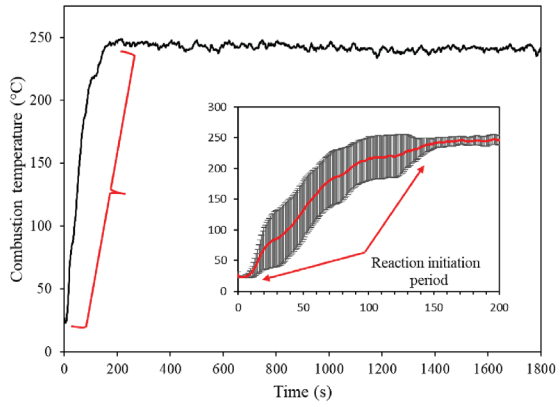

Figure 2: The combustion temperature profile of Pt/AAO catalyst at a hydrogen flow rate of 40 NmL min^{-1} for 30 min of CHC

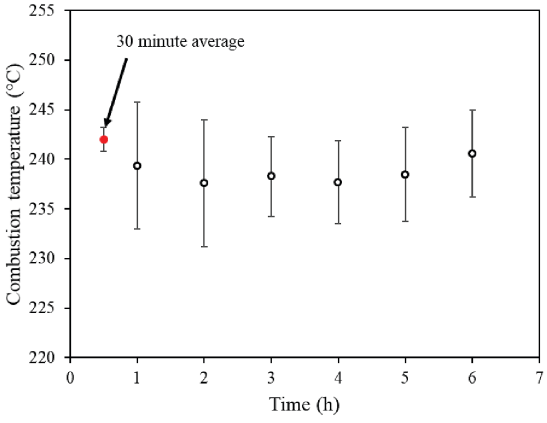

Figure 3: The 6h combustion temperature profile of Pt/AAO catalyst at a hydrogen flow rate of 40 NmL min^{-1}. The average combustion temperature obtained from the 30 min reactions was included in red

It is evident from Figure 3 that a relatively stable reaction temperature was maintained for the 6 h CHC reaction. The combustion temperature, calculated for each elapsed hour, ranged between 237 to 240 °C, and the standard deviation did not exceed 6.4%. In all cases, the combustion temperature per elapsed hour of combustion was slightly below the 30 min CHC reaction average value (indicated in red). This may be ascribed to the cooling effect of randomized local airflow (which caused temperature fluctuations), and considering that the combustion period was longer than for the 30 min CHC, the effect thereof on the average combustion temperature and standard deviation was more obvious. Furthermore, the stable combustion temperature observed in Figure 3 suggests that the majority of hydrogen (>99%) was consumed. It is accepted that some hydrogen slippage is inevitable. Fumey et al. showed that hydrogen slippage decreases with increasing burner temperature,[46] suggesting that a higher combustion temperature affords a higher rate of hydrogen recombination (Reaction 1). Nevertheless, considering hydrogen's low gaseous density, a build-up of hydrogen within a dwelling is highly unlikely and will dissipate before reaching an explosive concentration of 4 vol%.[47]

It may be concluded that Pt/AAO showed suitable reaction kinetics at 40 NmL min^{-1} hydrogen as a stable combustion temperature was achieved shortly after being exposed to hydrogen. The majority of hydrogen was consumed. The Pt/AAO catalysts were exposed to 20 to 140 NmL min^{-1} hydrogen flow rates to evaluate the effects of hydrogen flow rate on the combustion temperature. Figure 4 shows the combustion temperature profile of Pt/AAO at various hydrogen flow rates.

Figure 4 shows that the combustion temperature of the Pt/AAO catalyst increased near-linearly from 155 ± 2 to 467 ± 3 °C with an increase in the hydrogen flow rate from 20 to 120 NmL min^{-1}. Applying the equation shown in Figure 4, a 147 NmL min^{-1} hydrogen flow rate may facilitate a self-ignition temperature of 570 °C. The results presented in Figure 4 suggest that the Pt/AAO catalyst may be used for spatial heating, water boiling, or food preparation, as a relatively wide range of temperatures may be achieved by varying the hydrogen flow rate. However, it is crucial that during the development of a CHC-based cooker, the design thereof will be a significant factor to ensure proper heat transfer from the catalyst to the equipment that has to be heated.

Pt/AAO stability

Reduction in the activity of a catalytic system during high-temperature exposure is typically ascribed to catalyst aggregation – defined as the process whereby reactive metal particles agglomerate to form larger particles with a reduced reactive surface compared to non-agglomerated particles.[66] Catalyst aggregation is kinetically slow, typically occurring at more than 500 °C and accelerated in the presence of water vapour.[66] Catalyst aggregation can be prevented/limited if the reactive metal is supported on a suitable material. For instance, Du Preez et al. showed that a Pt thin layer forms large aggregates when supported on metallic Ti and stainless steel.[41, 49] Pt aggregation was significantly reduced by functionalizing the Ti and stainless steel to obtain native oxides of the two support materials. To evaluate the stability of the Pt/AAO catalyst, prolonged CHC was performed at 100 NmL min^{-1} hydrogen flow. Figure 5 shows the temperature profile of the prolonged CHC.

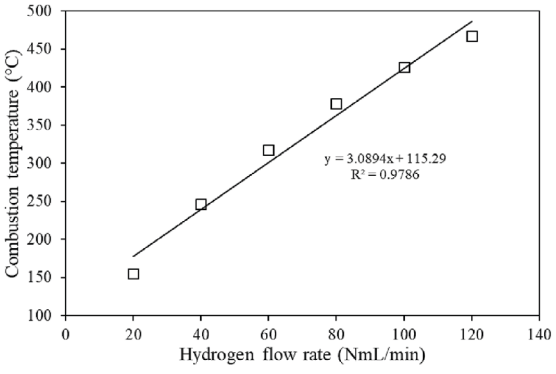

Figure 4: The effect of hydrogen flow rate on the combustion temperature of Pt/AAO

Figure 5 shows that a relatively stable combustion temperature of 408 ± 18 °C (based on 250 833 measurements, all data points included) could be maintained for 70 h of high-temperature CHC. Some deviations in the combustion temperature were observed – these are mainly ascribed to ambient temperature fluctuations in the day-night cycles. Also, irregular airflow and the associated cooling effects were observed and are ascribed to natural airflow and building ventilation (e.g., fume hoods). Kozhukhova et al. employed similar catalysts and obtained comparable combustion temperature profiles.[64, 67] Du Preez et al. performed the CHC reaction under similar conditions using different supports and obtained relatively similar combustion temperature profiles.[41, 49]

The stable combustion temperature observed in Figure 5 may indicate that catalyst aggregation was prevented or insignificant. To

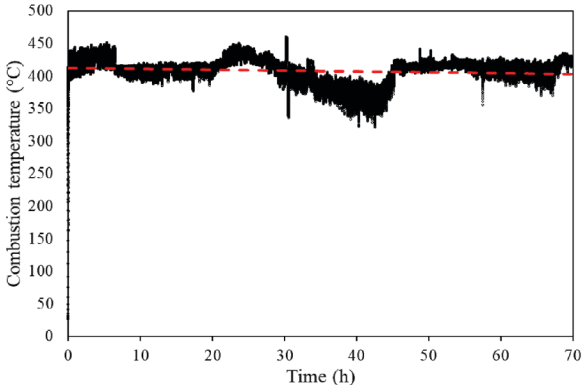

Figure 5. The combustion temperature profile of Pt/AAO catalyst at 100 NmL min^{-1} H_2 flow rate

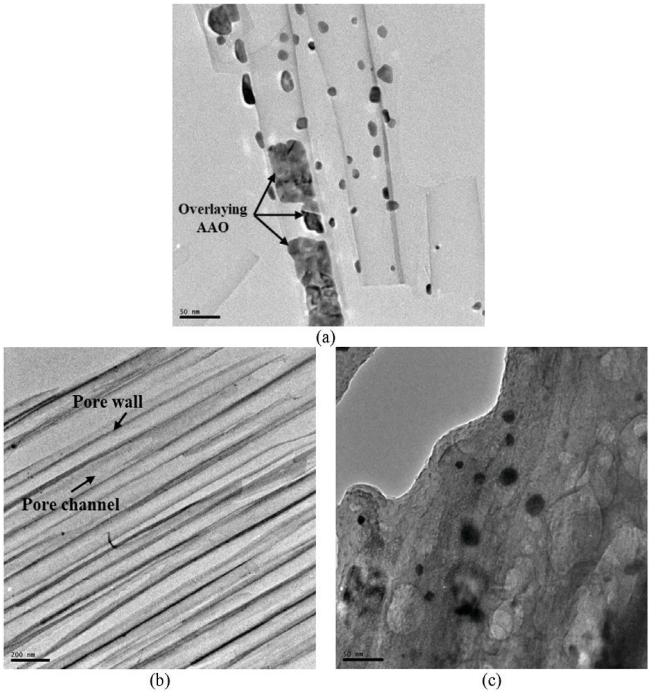

Figure 6: TEM image of Pt nanoparticles present on a section of mechanically separated AAO layer before the prolonged CHC procedure (a), a FIB cross-sectioned lamella of the AAO layer after the prolonged CHC procedure (b), and a representative area taken from (b) showing Pt nanoparticles

determine this, the Pt particle size before any and after prolonged CHC procedures were determined (Figure 6).

The particle size of the Pt particles shown in Figure 6a was 19.3 ± 9.6 nm. Some fractured AAO pieces formed during sample preparation and are indicated. These pieces can be identified as non-circular/randomly shaped. Figure 6b shows a FIB cross-sectioned lamella at low magnification and the pore walls and channels of the prepared AAO layer. The relatively disordered pore arrangement can be seen in Figure 6b, which was expected when considering Figure 1b. After the prolonged CHC procedure, the average Pt particle size of the particles presented in Figure 6c increased to 25.0 ± 4.6 nm. Though a relatively significant particle size increase was observed, the effect thereof on the catalytic activity of the Pt/AAO catalyst was not evident when considering Figure 5.

The bond energy between Pt and the support material affects the aggregation likelihood. Bartholomew stated that the rate of Pt aggregation of a Pt/Al_2O_3 is greater than that of a Ni/Al_2O_3 due to greater $Ni\text{-}Al_2O_3$ interaction.[66] A study by Kozhukhova et al. showed preliminary results that an AAO prepared by the anodization of a silicon-rich Al alloy could yield support suitable for CHC. Pt aggregation was insignificant after more than 500 h of CHC.[64] The combustion temperature obtained by Kozhukhova et al. was 338 ± 11 °C, which is slightly lower than the temperature presented in Figure 5. Nevertheless, catalyst aggregation was insignificant in both cases. It is proposed to evaluate prolonged CHC (>>70 h) using the catalyst prepared in this study in future research.

CONCLUSIONS

A nanostructured Pt/AAO catalyst, employable in prolonged CHC applications, was prepared. The applied anodization process preserved a metallic Al core at the centre of the catalyst support, which promoted heat displacement from reaction sites. By doing so, hot spot formation was mitigated, which lowered the likelihood of hydrogen's self-ignition.

It was determined that the CHC reaction became spontaneous after approximately 25 s of the catalyst being exposed to hydrogen under standard ambient conditions. The starting reaction temperature had a relatively significant effect on the initial temperature profile of the catalyst temperature profile - nevertheless, a stable combustion temperature of 408 ± 18 °C was maintained for 70 h. The average Pt particle size increased from 19.3 to 25.0 nm after the prolonged CHC procedure. This increase suggests that though some catalyst aggregation occurred, the adverse effect on the catalytic activity (i.e. combustion temperature) of the Pt/AAO catalyst was not evident.

ACKNOWLEDGMENTS

The Department of Science and Innovation (DSI), South Africa, and HySA Infrastructure Centre of Competence at the NWU, South Africa, are acknowledged for financial support through the KP5 program.

ORCID IDs

Stephanus P. du Preez – https://orcid.org/0000-0001-5214-3693
Alina E Kozhukhova – https://orcid.org/0000-0002-5709-5878
Dmitri G Bessarabov – https://orcid.org/0000-0001-6640-7573

REFERENCES

1. Lim SS, Vos T, Flaxman AD, Danaei G, Shibuya K, Adair-Rohani H, AlMazroa MA, Amann M, Anderson HR, Andrews KG, et al. A comparative risk assessment of burden of disease and injury attributable to 67 risk factors and risk factor clusters in 21 regions, 1990–2010: a systematic analysis for the Global Burden of Disease Study 2010. Lancet. 2012;380(9859):2224–2260. https://doi.org/10.1016/S0140-6736(12)61766-8.
2. Bonjour S, Adair-Rohani H, Wolf J, Bruce NG, Mehta S, Prüss-Ustün A, Lahiff M, Rehfuess EA, Mishra V, Smith KR. Solid fuel use for household cooking: country and regional estimates for 1980–2010. Environ Health Perspect. 2013;121(7):784–790. https://doi.org/10.1289/ehp.1205987.
3. WHO [World Health Organisation]. Household air pollution and health. https://www.who.int/news-room/fact-sheets/detail/household-air-pollution-and-health. 2021. [accessed 26 March 2021].
4. Naz S, Page A, Agho KE. Household air pollution and under-five mortality in Bangladesh (2004–2011). Int J Environ Res Public Health. 2015;12(10):12847–12862. https://doi.org/10.3390/ijerph121012847.
5. Dherani M, Pope D, Mascarenhas M, Smith KR, Weber M, Bruce N. Indoor air pollution from unprocessed solid fuel use and pneumonia risk in children aged under five years: a systematic review and meta-analysis. Bull World Health Organ. 2008;86(5):390–398C. https://doi.org/10.2471/BLT.07.044529.
6. Ranathunga N, Perera P, Nandasena S, Sathiakumar N, Kasturiratne A, Wickremasinghe R. Effect of household air pollution due to solid fuel combustion on childhood respiratory diseases in a semi urban population in Sri Lanka. BMC Pediatr. 2019;19(1):306. https://doi.org/10.1186/s12887-019-1674-5.
7. Taylor ET, Nakai S. Prevalence of acute respiratory infections in women and children in Western Sierra Leone due to smoke from wood and charcoal stoves. Int J Environ Res Public Health. 2012;9(6):2252–2265. https://doi.org/10.3390/ijerph9062252.
8. Jakubiak-Lasocka J, Lasocki J, Badyda AJ. Environmental Biomedicine. Cham: Springer; 2014. p. 39–48. https://doi.org/10.1007/5584_2014_93.
9. Das LM. Hydrogen-oxygen reaction mechanism and its implication to hydrogen engine combustion. Int J Hydrogen Energy. 1996;21(8):703–715. https://doi.org/10.1016/0360-3199(95)00138-7.
10. Saravanan N, Nagarajan G. An experimental investigation of hydrogen-enriched air induction in a diesel engine system. Int J Hydrogen Energy. 2008;33(6):1769–1775. https://doi.org/10.1016/j.ijhydene.2007.12.065.
11. Phillips R, Dunnill CW. Zero gap alkaline electrolysis cell design for renewable energy storage as hydrogen gas. RSC Advances. 2016;6(102):100643–100651. https://doi.org/10.1039/C6RA22242K.
12. Falch A, Badets VA, Labrugère C, Kriek RJ. Co-sputtered PtxPdyAlz thin film electrocatalysts for the production of hydrogen via SO2(aq) electro-oxidation. Electrocatalysis. 2016;7(5):376–390. https://doi.org/10.1007/s12678-016-0319-9.
13. Bessarabov DG, Human G, Kruger AJ, Chiuta S, Modisha PM, du Preez SP, Oelofse SP, Vincent I, Van Der Merwe J, Langmi HW, et al. South African hydrogen infrastructure (HySA infrastructure) for fuel cells and energy storage: overview of a projects portfolio. Int J Hydrogen Energy. 2017;42(19):13568–13588. https://doi.org/10.1016/j.ijhydene.2016.12.140.
14. Vincent I, Kruger A, Bessarabov D. Development of efficient membrane electrode assembly for low cost hydrogen production by anion exchange membrane electrolysis. Int J Hydrogen Energy. 2017;42(16):10752–10761. https://doi.org/10.1016/j.ijhydene.2017.03.069.
15. Vincent I, Bessarabov D. Low cost hydrogen production by anion exchange membrane electrolysis: A review. Renew Sustain Energy Rev. 2018;81:1690–1704. https://doi.org/10.1016/j.rser.2017.05.258.
16. Casallas C, Dincer I, Zamfirescu C. Experimental investigation and analysis of a novel photo-electrochemical hydrogen production cell with polymeric membrane photocathode. Int J Hydrogen Energy. 2016;41(19):7968–7975. https://doi.org/10.1016/j.ijhydene.2015.12.183.
17. Patel PP, Ghadge SD, Hanumantha PJ, Datta MK, Gattu B, Shanthi PM, Kumta PN. Active and robust novel bilayer photoanode architectures for hydrogen generation via direct non-electric bias induced photo-electrochemical water splitting. Int J Hydrogen Energy. 2018;43(29):13158–13176. https://doi.org/10.1016/j.ijhydene.2018.05.063.
18. Falch A, Kriek RJ. Laser induced H2 production employing Pt-TiO2 photocatalysts. J Photochem Photobiol Chem. 2013;271:117–123. https://doi.org/10.1016/j.jphotochem.2013.07.012.
19. Zhang J, Xing C, Shi F. MoS2/Ti3C2 heterostructure for efficient visible-light photocatalytic hydrogen generation. Int J Hydrogen Energy. 2020;45(11):6291–6301. https://doi.org/10.1016/j.ijhydene.2019.12.109.
20. Ziming C, Fuqiang W, Huaxu L, Shengpeng H, Bo L, Jianyu T, Hongyang L. Photon-absorption-based explanation of ultrasonic-assisted solar photochemical splitting of water to improve hydrogen production. Int J Hydrogen Energy. 2018;43(31):14439–14450. https://doi.org/10.1016/j.ijhydene.2018.06.037.
21. Liu W-S, Perng T-P. Ta2O5 hollow fiber composed of internal interconnected

mesoporous nanotubes and its enhanced photochemical H2 evolution. Int J Hydrogen Energy. 2019;44(33):17688–17696. https://doi.org/10.1016/j.ijhydene.2019.05.006.

22. Pandey B, Prajapati YK, Sheth PN. Recent progress in thermochemical techniques to produce hydrogen gas from biomass: A state of the art review. Int J Hydrogen Energy. 2019;44(47):25384–25415. https://doi.org/10.1016/j.ijhydene.2019.08.031.
23. Canavesio C, Nassini D, Nassini HE, Bohé AE. Study on an original cobalt-chlorine thermochemical cycle for nuclear hydrogen production. Int J Hydrogen Energy. 2020;45(49):26090–26103. https://doi.org/10.1016/j.ijhydene.2019.08.137.
24. Du Preez SP, Bessarabov DG. Hydrogen generation by means of hydrolysis using activated Al-In-Bi-Sn composites for electrochemical energy applications. Int J Electrochem Sci. 2017;12:8663–8682. https://doi.org/10.20964/2017.09.22.
25. Du Preez SP, Bessarabov DG. Hydrogen generation of mechanochemically activated Al-Bi-In composites. Int J Hydrogen Energy. 2017;42(26):16589–16602. https://doi.org/10.1016/j.ijhydene.2017.05.211.
26. Xiao F, Guo Y, Li J, Yang R. Hydrogen generation from hydrolysis of activated aluminum composites in tap water. Energy. 2018;157:608–614. https://doi.org/10.1016/j.energy.2018.05.201.
27. Du Preez SP, Bessarabov DG. Hydrogen generation by the hydrolysis of mechanochemically activated aluminum-tin-indium composites in pure water. Int J Hydrogen Energy. 2018;43(46):21398–21413. https://doi.org/10.1016/j.ijhydene.2018.09.133.
28. Sekoai PT, Ouma CNM, du Preez SP, Modisha P, Engelbrecht N, Bessarabov DG, Ghimire A. Application of nanoparticles in biofuels: an overview. Fuel. 2019;237:380–397. https://doi.org/10.1016/j.fuel.2018.10.030.
29. Du Preez SP, Bessarabov DG. The effects of bismuth and tin on the mechanochemical processing of aluminum-based composites for hydrogen generation purposes. Int J Hydrogen Energy. 2019;44(39):21896–21912. https://doi.org/10.1016/j.ijhydene.2019.06.154.
30. Du Preez SP, Bessarabov DG. Material aspects pertaining to hydrogen production from aluminum: opinion. Research and Development in Material Sciences. 2019;12(1). https://doi.org/10.31031/RDMS.2019.12.000778.
31. Du Preez SP. Hydrogen generation by the reaction of mechanochemically activated aluminium and water [PhD thesis]. Potchefstroom: North-West University. 2019.
32. Du Preez SP, Bessarabov DG. On-demand hydrogen generation by the hydrolysis of ball-milled aluminum composites: A process overview. Int J Hydrogen Energy. 2021;46(72):35790–35813. https://doi.org/10.1016/j.ijhydene.2021.03.240.
33. Balat M. Potential importance of hydrogen as a future solution to environmental and transportation problems. Int J Hydrogen Energy. 2008;33(15):4013–4029. https://doi.org/10.1016/j.ijhydene.2008.05.047.
34. Damyanova S, Pawelec B, Arishtirova K, Fierro J. Ni-based catalysts for reforming of methane with CO_2. Int J Hydrogen Energy. 2012;37(21):15966–15975. https://doi.org/10.1016/j.ijhydene.2012.08.056.
35. White R, Feldman R, Proctor S. Neurobehavioral effects of toxic exposures, clinical syndromes in adult neuropsychology: the practitioners handbook. White RF, editor. Amsterdam: Elsevier; 1992. p. 1–51.
36. Townsend C, Maynard R. Effects on health of prolonged exposure to low concentrations of carbon monoxide. Occup Environ Med. 2002;59(10):708–711. https://doi.org/10.1136/oem.59.10.708.
37. Prockop LD, Chichkova RI. Carbon monoxide intoxication: an updated review. J Neurol Sci. 2007;262(1-2):122–130. https://doi.org/10.1016/j.jns.2007.06.037.
38. Best R, Burke PJ. Electricity availability: A precondition for faster economic growth? Energy Econ. 2018;74:321–329. https://doi.org/10.1016/j.eneco.2018.06.018.
39. Amankwah-Amoah J. Solar energy in sub-Saharan Africa: The challenges and opportunities of technological leapfrogging. Thunderbird Int Bus Rev. 2015;57(1):15–31. https://doi.org/10.1002/tie.21677.
40. Turner JA. A realizable renewable energy future. Science. 1999;285(5428):687–689. https://doi.org/10.1126/science.285.5428.687.
41. Du Preez SP, Jones DR, Warwick MEA, Falch A, Sekoai PT, Mota das Neves Quaresma C, Bessarabov DG, Dunnill CW. C. Mota das Neves Quaresma, D. G. Bessarabov, C. W. Dunnill, Thermally stable Pt/Ti mesh catalyst for catalytic hydrogen combustion. Int J Hydrogen Energy. 2020;45(33):16851–16864. https://doi.org/10.1016/j.ijhydene.2020.04.112.
42. Judd R, Pinchbeck D. Offering a solution to the energy storage problem. Cambridge: Woodhead Publishing. 2013.
43. Bessarabov D, Millet P. PEM water electrolysis. Vol. 1. London: Academic Press; 2018.
44. İlbas M, Yılmaz İ, Kaplan Y. Investigations of hydrogen and hydrogen–hydrocarbon composite fuel combustion and NOx emission characteristics in a model combustor. Int J Hydrogen Energy. 2005;30(10):1139–1147. https://doi.org/10.1016/j.ijhydene.2004.10.016.
45. Frassoldati A, Faravelli T, Ranzi E. A wide range modeling study of NOx formation and nitrogen chemistry in hydrogen combustion. Int J Hydrogen Energy. 2006;31(15):2310–2328. https://doi.org/10.1016/j.ijhydene.2006.02.014.
46. Fumey B, Buetler T, Vogt UF. Ultra-low NOx emissions from catalytic hydrogen combustion. Appl Energy. 2018;213:334–342. https://doi.org/10.1016/j.apenergy.2018.01.042.
47. Du Toit MH, Avdeenkov AV, Bessarabov D. Reviewing H2 combustion: a case study for non-fuel-cell power systems and safety in passive autocatalytic recombiners. Energy Fuels. 2018;32(6):6401–6422. https://doi.org/10.1021/acs.energyfuels.8b00724.
48. Saint-Just J, Etemad S. Compendium of Hydrogen Energy. Barbir F, Basile A, Veziroğlu TN, editors. Oxford: Woodhead Publishing; 2016. p. 263–287. https://doi.org/10.1016/B978-1-78242-363-8.00010-4.
49. Du Preez SP, Jones DR, Bessarabov DG, Falch A, Mota das Neves Quaresma C, Dunnill CW. C. Mota das Neves Quaresma, C. W. Dunnill, Development of a Pt/stainless steel mesh catalyst and its application in catalytic hydrogen combustion. Int J Hydrogen Energy. 2019;44(49):27094–27106. https://doi.org/10.1016/j.ijhydene.2019.08.168.
50. Kozhukhova AE, du Preez SP, Bessarabov DG. Catalytic hydrogen combustion for domestic and safety applications: a critical review of catalyst materials and technologies. Energies. 2021;14(16):4897. https://doi.org/10.3390/en14164897.
51. Kozhukhova AE, du Preez SP, Bessarabov DG. Preparation of anodized aluminium oxide at high temperatures using low purity aluminium (Al6082). Surf Coat Tech. 2019;378:124970. https://doi.org/10.1016/j.surfcoat.2019.124970.
52. Kozhukhova AE, du Preez SP, Bessarabov DG. The effects of pore widening and calcination on anodized aluminum oxide prepared from Al6082. Surf Coat Tech. 2020;383:125234. https://doi.org/10.1016/j.surfcoat.2019.125234.
53. Vojkuvka L, Marsal LF, Ferré-Borrull J, Formentin P, Pallarés J. Self-ordered porous alumina membranes with large lattice constant fabricated by hard anodization. Superlattices Microstruct. 2008;44(4-5):577–582. https://doi.org/10.1016/j.spmi.2007.10.005.
54. Schneider CA, Rasband WS, Eliceiri KW. NIH Image to ImageJ: 25 years of image analysis. Nat Methods. 2012;9(7):671–675. https://doi.org/10.1038/nmeth.2089.
55. Fumey B, Stoller S, Fricker R, Weber R, Dorer V, Vogt UF. Development of a novel cooking stove based on catalytic hydrogen combustion. Int J Hydrogen Energy. 2016;41(18):7494–7499. https://doi.org/10.1016/j.ijhydene.2016.03.134.
56. Feng B, Li Z, Zhang X. Prediction of size effect on thermal conductivity of nanoscale metallic films. Thin Solid Films. 2009;517(8):2803–2807. https://doi.org/10.1016/j.tsf.2008.10.116.
57. Živcová Z, Gregorová E, Pabst W, Smith DS, Michot A, Poulier C. Thermal conductivity of porous alumina ceramics prepared using starch as a pore-forming agent. J Eur Ceram Soc. 2009;29(3):347–353. https://doi.org/10.1016/j.jeurceramsoc.2008.06.018.
58. Miao Q, Xiong G, Sheng S, Cui W, Xu L, Guo X. Partial oxidation of methane to syngas over nickel-based catalysts modified by alkali metal oxide and rare earth metal oxide. Appl Catal A Gen. 1997;154(1-2):17–27. https://doi.org/10.1016/S0926-860X(96)00377-8.
59. McCarty JG, Gusman M, Lowe DM, Hildenbrand DL, Lau KN. Stability of supported metal and supported metal oxide combustion catalysts. Catal Today. 1999;47(1-4):5–17. https://doi.org/10.1016/S0920-5861(98)00279-X.
60. Kim SC. The catalytic oxidation of aromatic hydrocarbons over supported

metal oxide. J Hazard Mater. 2002;91(1-3):285–299. https://doi.org/10.1016/S0304-3894(01)00396-X.

61. Lyubovsky M, Pfefferle L. Methane combustion over the α-alumina supported Pd catalyst: activity of the mixed Pd/PdO state. Appl Catal A Gen. 1998;173(1):107–119. https://doi.org/10.1016/S0926-860X(98)00149-5.
62. Lyubovsky M, Pfefferle L, Datye A, Bravo J, Nelson T. TEM Study of the Microstructural modifications of an alumina-supported palladium combustion catalyst. J Catal. 1999;187(2):275–284. https://doi.org/10.1006/jcat.1999.2545.
63. Deutschmann O, Maier LI, Riedel U, Stroemman AH, Dibble RW. Hydrogen assisted catalytic combustion of methane on platinum. Catal Today. 2000;59(1-2):141–150. https://doi.org/10.1016/S0920-5861(00)00279-0.
64. Kozhukhova AE, du Preez SP, Shuro I, Bessarabov DG. Development of a low purity aluminum alloy (Al6082) anodization process and its application as a platinum-based catalyst in catalytic hydrogen combustion. Surf Coat Tech. 2020;404:126483. https://doi.org/10.1016/j.surfcoat.2020.126483.
65. Naicker N, Teare J, Balakrishna Y, Wright CY, Mathee A. Indoor temperatures in low cost housing in Johannesburg, South Africa. Int J Environ Res Public Health. 2017;14(11):1410. https://doi.org/10.3390/ijerph14111410.
66. Bartholomew CH. Mechanisms of catalyst deactivation. Appl Catal A Gen. 2001;212(1-2):17–60. https://doi.org/10.1016/S0926-860X(00)00843-7.
67. Kozhukhova AE, du Preez SP, Malakhov AA, Bessarabov DG. A thermally conductive Pt/AAO catalyst for hydrogen passive autocatalytic recombination. Catalysts. 2021;11(4):491. https://doi.org/10.3390/catal11040491.